Three-Dimensional Lanthanoid-Containing Coordination Frameworks: Structure, Magnetic and Fluorescent Properties

Hong-Tao Zhang,[a] You Song,[a] Yong-Xiu Li,[a] Jing-Lin Zuo,[a] Song Gao,[b] and Xiao-Zeng You*[a]

Keywords: Lanthanides / Coordination polymers / Magnetic properties / Fluorescence / Solid-state structures

Two lanthanoid-containing 3D coordination polymers, $[Gd_2L_3(H_2O)_2]_n$ (**1**) and $\{[TbL_{1.5}(H_2O)]\cdot 0.5H_2O\}_n$ (**2**) (L = succinate), have been prepared by hydrothermal reaction. The difference in structure between the two 3D coordination polymers is a result of the flexibility of the ligand conformation. The magnetic properties of **1** and **2** have been investigated in the 1.8–300 K range. Both complexes exhibit ferromagnetic interaction between lanthanoid ions. AC magnetic measurements revealed long-range magnetic order in complex **2**. Especially **2** integrates the ferromagnetic, fluorescent and porous properties into a single entity. This motif may be developed to achieve new multifunctional molecular-based materials.

Introduction

Solid-state assembly of coordination polymers has attracted increasing attention due to their fascinating structure as well as their potential applications in materials science, such as zeolite-like porous structures and optoelectronic properties.[1,2] To construct coordination polymers, polydentate organic ligands are usually employed as space linkers to connect the metal ions.[3,4] The resultant functionality might not only rise from the organic ligand molecules but also from the inorganic metal ions. Accordingly, the wide-ranging functionality of the metal moiety, such as magnetic and optoelectronic properties, can be associated with the ability of the organic ligands to modulate special structural arrangements, to develop new molecular-based materials. Moreover, this supramolecular entity could lead to a multifunctional materials.[5] For this purpose, more new unique 3d- and 4f-metal containing coordination polymers have been investigated.[6–11] Most work involving lanthanoids has focused on the structures and luminescent properties of the complexes rather than on magnetic properties. In these lanthanoid-containing coordination polymers, many organic ligands containing oxygen atoms are employed as a bridge to connect the lanthanoid ions because of the high affinity of the lanthanoid ions for oxygen-containing ligands, such as the terephthalate anion[11d] and 4,4′-bipyridine *N*,*N*′-dioxide.[11a,b] Among them, aromatic polycarboxylate anions are widely used because of their rigid structure.[8,11] However, the structural variation of coordination polymers is ascribed to both the metal–ligand coordination modes and the conformational isomerism of ligands that arises from their flexibility. Generally, for aliphatic carboxylate ligands, the conformational variation of flexibility plays a more remarkable role than that in aromatic carboxylate ligands. As a simple aliphatic dicarboxylate ligand with multi-conformation isomerism, the succinate anions is the better choice to investigate the effect of conformational variation in coordination polymers because of the uncomplicated results. To date, in (succinato)metal coordination polymers, the inorganic species are mostly d-block metals such as Fe^{II} succinate[12d] and several (succinato)cobalt(II) coordination polymers with different structures.[12a–c] Recently, a few (succinato)nickel(II) coordination polymers as porous materials and one example of a (succinato)Sc^{III} 3D coordination polymer as a heterogeneous Lewis acid catalyst have been reported.[13,14] There are only two examples of lanthanoid coordination polymers involving succinate, praseodymium succinate [15a] and lutetium succinate.[15b] In this paper, we present two 3D lanthanoids coordination frameworks, $[Gd_2L_3(H_2O)_2]_n$ (**1**) (L = succinate) and $\{[TbL_{1.5}(H_2O)]\cdot 0.5H_2O\}_n$ (**2**), both of which exhibit ferromagnetic interaction between lanthanoid ions. Moreover, **2** emits an intense green fluorescence in the solid state at room temperature.

[a] State Key Laboratory of Coordination Chemistry, Nanjing University,
Nanjing 210093, China
E-mail: xyz@netra.nju.edu.cn
[b] State Key Laboratory of Rare Earth Materials Chemistry and Applications, Peking University,
Beijing 100871, China

  DOI: 10.1002/ejic.200400376

Results and Discussion

Crystal Structures

[$Gd_2L_3(H_2O)_2$]$_n$ (1)

A single-crystal X-ray analysis revealed that the solid-state structure of gadolinium(III) succinate differs from that of previously reported praseodymium(III) succinate and lutetium succinate. There are two crystallographically independent gadolinium ions in the asymmetric unit (Figure 1a). Each gadolinium ion is ninefold coordinated by eight oxygen atoms from carboxylate groups of six succinate ions and one oxygen atom from the water molecule. Gd–O bond lengths vary in the range 2.357(8)–2.562(9) Å – in agreement with those of previously reported carboxylate-containing gadolinium complexes (2.308–2.597 Å).[9c] Table 1 gives selected bond lengths and angles. Two Gd^{III} ions are connected by three carboxylate groups, in which one acts as a carboxylate bridge in the usual $\eta^1:\eta^1:\mu_2$ mode while the other two serve as oxo-carboxylate bridges in the less common $\eta^2:\eta^1:\mu_2$ fashion.[9a] Along the *a* axis, the edge-sharing GdO_9 polyhedra extend to a 1D metal oxide like zigzag chain. In the chain, the metal–metal separation for the two symmetrically independent gadolinium ions Gd1–Gd2 is 4.0583(12) Å. The distance between two adjacent symmetrically related Gd^{III} ions is slightly elongated to 4.0595(13) Å [Gd1–Gd2^{I} (I: 1 + *x*, *y*, *z*) or Gd2–Gd1^{II} (II: *x* – 1, *y*, *z*)]. In the lattice, all metal oxide like chains are connected through the carbon–hydrogen chains of the succinate ions to produce 3D lanthanoid coordination frameworks. Notably, there are three conformations in the carbon–hydrogen chains of succinates, which can be observed along the *a* axis (Figure 2). Two of them adopt *gauche*-staggered conformations and extend along the *c* axis, approximately. One such conformation has a torsion angle of 89.5(12)° (C9–C10–C11^{III}–C12^{III}, III: 1 – *x*, 2 – *y*, 1 – *z*) and the other of 70.7(13)° (C5–C6–C7^{IV}–C8^{IV}, IV: 1 – *x*, 2 – *y*, 2 – *z*). The third succinato ligand possesses an *anti*-staggered conformation and extends along the *b* axis, approximately. Here, both carboxylate groups serve as $\eta^2:\eta^1:\mu_2$ mode bridges. In the *gauche*-staggered conformations, however, one carboxylate ion acts as a carboxylate bridge in $\eta^1:\eta^1:\mu_2$ fashion and another as a $\eta^2:\eta^1:\mu_2$ mode bridge.

Table 1. Selected bond lengths [Å], angles [°] and torsion angles [°] for **1**

Gd(1)–O(12)	2.358(9)	Gd(1)–O(7)	2.378(8)
Gd(1)–O(10)	2.454(9)	Gd(1)–O(1W)	2.457(11)
Gd(1)–O(3)[a]	2.461(9)	Gd(1)–O(2)	2.462(10)
Gd(1)–O(5)[a]	2.467(9)	Gd(1)–O(1)	2.474(8)
Gd(1)–O(9)	2.514(8)	Gd(2)–O(6)	2.357(8)
Gd(2)–O(2W)	2.402(9)	Gd(2)–O(11)	2.412(9)
Gd(2)–O(9)	2.419(8)	Gd(2)–O(1)[b]	2.427(9)
Gd(2)–O(8)	2.458(8)	Gd(2)–O(4)	2.483(10)
Gd(2)–O(3)	2.537(9)	Gd(2)–O(7)	2.562(9)
O(12)–Gd(1)–O(7)	75.8(3)	O(12)–Gd(1)–O(10)	75.2(4)
O(7)–Gd(1)–O(10)	119.3(3)	O(12)–Gd(1)–O(1W)	78.1(4)
O(12)–Gd(1)–O(3)[a]	139.7(3)	O(7)–Gd(1)–O(3)[a]	142.8(3)
O(12)–Gd(1)–O(2)	75.7(3)	O(12)–Gd(1)–O(5)[a]	142.2(3)
O(12)–Gd(1)–O(1)	125.4(3)	O(7)–Gd(1)–O(1)	101.3(3)
O(2W)–Gd(2)–O(1)[b]	142.7(3)	O(6)–Gd(2)–O(8)	79.0(3)
O(11)–Gd(2)–O(4)	113.7(4)	O(9)–Gd(2)–O(4)	75.2(3)
O(9)–Gd(2)–O(3)	99.7(3)	O(8)–Gd(2)–O(3)	140.6(3)
O(6)–Gd(2)–O(7)	124.6(3)	O(2W)–Gd(2)–O(7)	72.2(3)
O(3)–Gd(2)–O(7)	155.9(3)	C(9)–C(10)–C(11)[d]–C(12)[d]	89.4(12)
C(5)–C(6)–C(7)[c]–C(8)[c]	–70.7(14)	C(1)–C(2)–C(3)[e]–C(4)[e]	178.8(11)

Symmetry transformations used to generate equivalent atoms: [a] (I): *x* + 1, *y*, *z*. [b] (II): *x* – 1, *y*, *z*. [c] (III): –*x* + 1, –*y* + 2, –*z* + 2. [d] (IV): –*x* + 1, –*y* + 2, –*z* + 1. [e] (V): *x* + 2, *y* – 1, *z*.

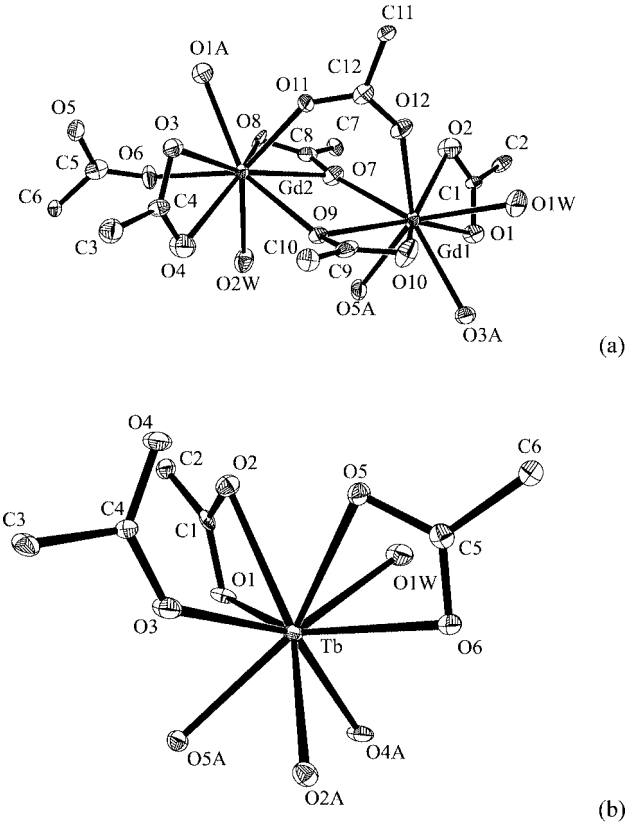

Figure 1. (a) Coordination environment of the complex [$Gd_2L_3(H_2O)_2$]$_n$ (**1**) with ellipsoids drawn at 50% probability level; for clarity, all hydrogen atoms are omitted and only the asymmetric half of the succinato ligand is shown; symmetry code: (A) = *x* + 1, *y*, *z*; (b) coordination environment of **2**; lattice water molecule and all hydrogen atoms omitted for clarity, and thermal ellipsoids shown at 50% probability; symmetry code: (A) = –*x* + ½, *y* – ½, –*z* + ½

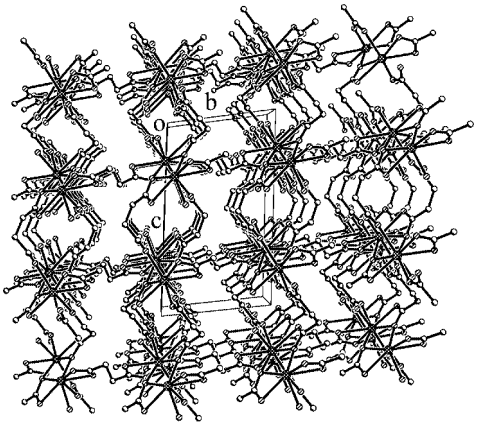

Figure 2. 3D framework of **1** projected down the 1D chain; hydrogen atoms omitted for clarity

{[TbL$_{1.5}$(H$_2$O)]·0.5H$_2$O}$_n$ (2)

Complex **2** also has a 3D framework, but differs from complex **1**, containing a mononuclear asymmetric unit that consists of a terbium(III) ion, a coordinating water molecule, 1½ succinate ions as well as ½ a guest water molecule. The terbium(III) ion is also ninefold coordinated by eight oxygen atoms from six carboxylate groups and one water oxygen atom. All oxygen atoms around the Tb^{III} ion form a TbO_9 unit that can be viewed as a tricapped trigonal prism. Tb–O bond lengths are in the range 2.294(4)–2.507(4) Å, which are consistent with that of a previously reported carboxylate-containing terbium complex [2.264(6)–2.533(6) Å].[7b] Table 2 gives selected bond lengths and angles. Along the *b* axis, the TbO_9 polyhedra extend to a 1D zigzag chain by sharing the polyhedron edge. The 1D metal oxide like chains are linked by carbon chains of the ligands to form a 3D metal-organic framework (3D MOF). Although the succinato ligands function in the same modes as in **1**, there are 1D channels that include guest water molecules in the 3D MOF and only one Tb···Tb separation [4.0211(5) Å] in the metal oxide like chains. Guest water molecules are bound to the framework through weak hydrogen bonds, O(2W)–H(2WB)···O(1W) (Table 3). However, the conformations of the carbon–hydrogen chains of the succinato ligands differ slightly from that of **1**. There are just two conformations of the carbon chains in **2** (Figure 3), a *gauche*-staggered with a torsion angle of 72.8(7)° (C1–C2–$C3^V$–$C4^V$, V: x, $y - 1$, $z - 0.5$) and an *anti*-staggered (Table 2). Therefore, the host structural difference between the two complexes is probably caused by the flexibility of the ligand.

Table 2. Selected bond lengths [Å], angles [°] and torsion angles [°] for **2**

Tb(1)–O(4)[a]	2.294(4)	Tb(1)–O(2)[a]	2.395(4)
Tb(1)–O(5)[a]	2.398(4)	Tb(1)–O(3)	2.416(4)
Tb(1)–O(5)	2.441(4)	Tb(1)–O(1W)	2.456(4)
Tb(1)–O(6)	2.462(5)	Tb(1)–O(1)	2.465(4)
Tb(1)–O(2)	2.507(4)	O(4)[a]–Tb(1)–O(2)[a]	77.13(14)
O(4)[a]–Tb(1)–O(5)[a]	75.80(14)	O(2)[a]–Tb(1)–O(5)[a]	68.55(14)
O(4)[a]–Tb(1)–O(6)	85.74(15)	O(2)[a]–Tb(1)–O(6)	71.48(14)
O(4)[a]–Tb(1)–O(1)	82.66(15)	O(2)[a]–Tb(1)–O(1)	137.65(13)
O(2)[a]–Tb(1)–O(2)	152.63(4)	O(5)[a]–Tb(1)–O(2)	104.77(14)
O(3)–Tb(1)–O(2)	78.11(13)	O(5)–Tb(1)–O(2)	66.13(14)
O(1W)–Tb(1)–O(2)	71.45(13)	O(6)–Tb(1)–O(2)	115.54(13)
O(1)–Tb(1)–O(2)	51.65(13)	C(1)–C(2)–C(3)[b]–C(4)[b]	72.8(7)
C(4)–C(3)–C(2)[c]–C(1)[c]	–72.8(7)	C(5)–C(6)–C(6)[d]–C(5)[d]	180.000(1)

Symmetry transformations used to generate equivalent atoms: [a] (I): $-x + 1/2$, $y - 1/2$, $-z + 1/2$. [b] (III): x, $-y + 1$, $z - 1/2$. [c] (IV): x, $-y + 1$, $z + 1/2$. [d] (V): $-x + 1$, $-y + 1$, $-z + 1$.

Table 3. Hydrogen bonds for **2**

D–H···A	*d*(D–H) [Å]	*d*(H···A) [Å]	*d*(D···A) [Å]	<(DHA) [°]
O(1W)–H(1WB)···O(3)[a]	0.85	2.14	2.853(6)	141.4
O(1W)–H(1WA)···O(1)[b]	0.85	1.86	2.707(6)	173.4
O(2W)–H(2WB)···O(1W)	0.85	2.22	2.927(5)	140.5

Symmetry transformations used to generate equivalent atoms: [a] (II): $-x + 1/2$, $y + 1/2$, $-z + 1/2$. [b] (VI): $-x + 1/2$, $-y + 1/2$, $-z$.

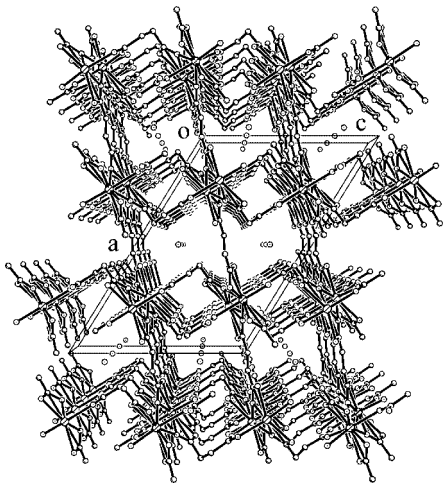

Figure 3. 1D channels including guest water molecules in the 3D frameworks of **2**; all hydrogen atoms omitted for clarity

Thermal Properties

Thermal gravimetric analysis (TGA) is consistent with the X-ray structural results of both coordination polymers. For complex **1**, the gradual weight loss from 115 to 197 °C (5.35%) corresponds to the loss of coordination water molecules (calcd. 5.16%). The complex then decomposes above 404 °C. In contrast, complex **2** shows a sharp weight loss in the range 86–94 °C (3.26%) due to the loss of the guest water (calcd. 2.50%). The thermal analysis curve confirms the presence of guest molecules in the channels of the 3D MOF containing terbium. The second weight-loss (156–202 °C, 5.52%) can be attributed to the loss of coordination water molecules (calcd. 5.13%). Complex **2** decomposes above 400 °C.

Magnetic Properties

The magnetic behavior of complex **1** is represented in Figure 4 as $\chi_M T$ vs. T. At room temperature, $\chi_M T$ is 15.55 $cm^3\,mol^{-1}\,K$, which is close to the value, 15.75 $cm^3\,mol^{-1}\,K$, of two non-interacting Gd^{3+} ions in the $^8S_{7/2}$ ground state. With decreasing temperature, $\chi_M T$ decreases smoothly and reaches a minimum of 15.17 $cm^3\,mol^{-1}$ at 50 K. Below this temperature, $\chi_M T$ increases rapidly, indicating that the ferromagnetic interaction between the Gd^{3+} ions dominates the magnetic properties of complex **1**. This overall feature indicates two conflicting effects. Ferromagnetic interaction between two Gd^{3+} ions increases the molecular magnetism, while some other factors induce the decrease of $\chi_M T$. Similar behavior observed in other lanthanoid-containing complexes[8b,9e] is suggested to arise from the Stark effect caused by the crystal-field perturbation and splitting f orbits. This effect tends to lower the local contributions of the lanthanoid ions.[16] However, the Gd^{3+} ion has a half-filled 4f shell and, to a first approximation, its ground state must not split in ligand fields. Actually, the crystal field distorts the ion symmetry and the degeneracy is broken partly, and a slight splitting always

occurs. Generally, the Stark effect for Gd^{III} is of the order of 0.05 cm^{-1}, which is not enough to decrease $\chi_M T$ in the range 50–300 K. In both $GdCl_3$ and $Gd(OH)_3$, both ferromagnetic and antiferromagnetic interactions are present. They arise from the usual Heisenberg form of the exchange plus magnetic-dipole interaction and they do not change appreciably below 77 K.[17–19] The nearest-neighbor (J_{nn}) interactions (*nn* pairs) are antiferromagnetic while those of the next-nearest neighbor (J_{nnn}) interactions (*nnn* pairs) are ferromagnetic. The observed magnetic behavior depends on the dominant interaction. The description of this system closely follows the spin-wave theory used successfully for 3d ions.[19] In complex **1**, the two Gd–Gd separations mentioned above probably make the *nn* and *nnn* pairs, such as Gd1–Gd2 and Gd2–Gd1′. The *nnn* pairs could not, seemingly, be Gd1–Gd1′ or Gd2–Gd2′, because the shortest distance between them is ca. 7.707 Å. Interaction at this distance should be very weak and could be neglected. However, it could not be confirmed as intrinsic source. The nature of the Gd···Gd interaction in **1** is supported by magnetization measurements in the 0–7 T range at 1.83 K. The magnetization plot per Gd^{3+} ion closely follows the Brillouin function with a theoretical *g* factor (g = 2.0) (Figure 5).[20]

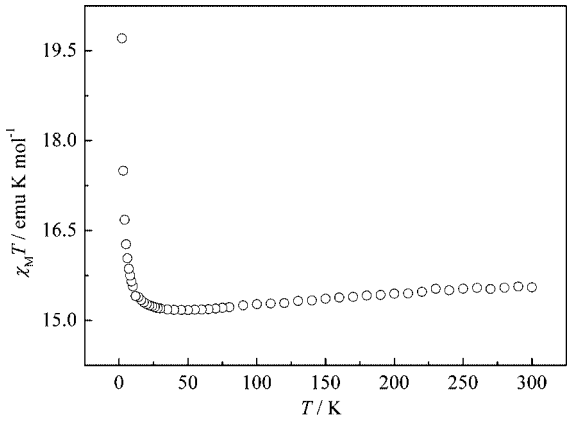

Figure 4. Temperature dependence of $\chi_M T$ for **1**

For complex **2**, $\chi_M T$ increases with decreasing temperature over the whole temperature range (Figure 6), implying that ferromagnetic coupling between Tb^{3+} ions dominates the magnetic properties. At room temperature, $\chi_M T$ is 23.10 $cm^3\ mol^{-1}$ K, which is close to the value of two non-interacting Tb^{3+} ions in the $^7F_6$ ground state (11.82 $cm^3\ mol^{-1}$ per Tb^{3+} ion).[20] $\chi_M T$ increases steadily from 300 to 20 K, and then increases rapidly on further cooling to 1.8 K. All these data indicate a ferromagnetic interaction between two terbium ions in **2**. AC magnetic measurements show a strong temperature dependence of both in-phase magnetization, χ', and out-of-phase magnetization, χ''. Both χ' and χ'' sharply increase below 4 K, suggesting long-range ordering in **1**. The ordering temperature is <1.8 K because no peaks are observed in χ' and χ'' vs. T plots (Figure 7). This appears to be the first observation of long-range ordering in fully structurally characterized lanthanoid-containing coordination compounds that display a ferromagnetic interaction.

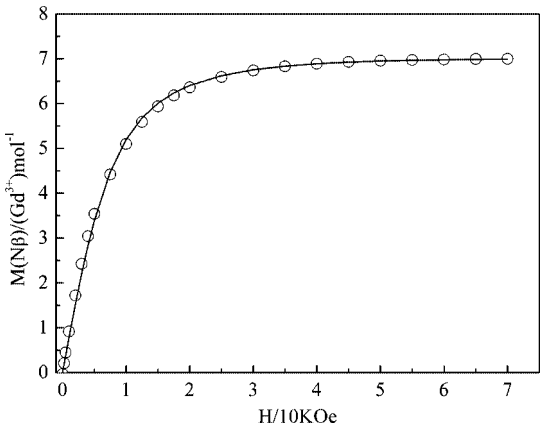

Figure 5. Field dependence of the magnetization for **1** at 1.83 K (circles); the solid line represents the Brillouin function for two magnetically isolated Gd^{III} ions with g = 2.0

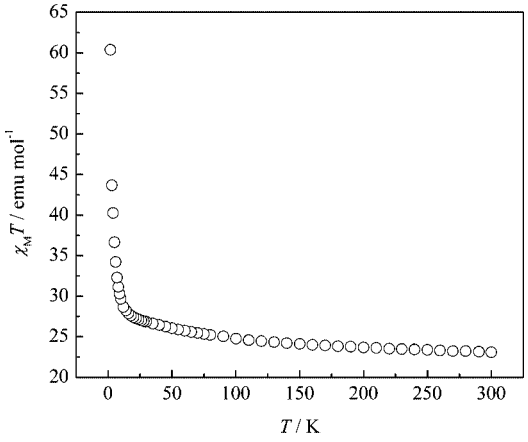

Figure 6.Temperature dependence of $\chi_M T$ for **2**

The magnetic properties of most lanthanoid ions are strongly influenced by their rather large unquenched orbital angular momentum associated with the internal nature of the valence f orbits.[20] This is one reason why lanthanoid compounds are widely applied in magnet technology, but also accounts for the difficulty in studying their magnetic properties. Recent interest has focused on the magnetic behavior of the f-block coordination compounds.[8–10,21] Only two examples of well-characterized lanthanoid complexes containing gadolinium display ferromagnetic interaction between lanthanoid ions;[9c,d] others have observed ferromagnetism in dinuclear triple-decker complexes that include Tb, Dy and Ho, but without structural characterization.[21] The ferromagnetic interaction observed here in the gadolinium carboxylate compound probably arises from the accidental orthogonality between the magnetic orbitals of the two interacting Gd^{III} ions, the angle at the oxo bridge, and the Gd···Gd separation through it.[9c]

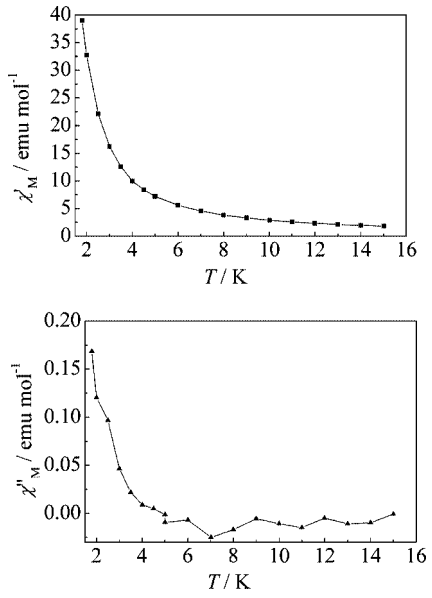

Figure 7. χ'_M(top) and χ''_M (bottom) vs. T, where χ'_M and χ''_M are in-phase-AC and out-of-phase-AC molar magnetic susceptibilities, respectively

Fluorescent Properties

Complex **2** emits an intense green light in the solid state at room temperature. Excitation and emission spectra (Figure 8) show typical Tb^{III} excitation peaks at 319 ($^7F_6 \rightarrow {}^5D_0$), 342 ($^7F_6 \rightarrow {}^5L_7$), 352 ($^7F_6 \rightarrow {}^5L_9$), 370 ($^7F_6 \rightarrow {}^5G_5$) and 379 nm ($^7F_6 \rightarrow {}^5G_6$), indicating that direct excitation of the terbium ion operates in complex **2** when emission at 544 nm is observed. The emission spectra are almost identical when excited at 352 and 370 nm. Emission peaks at 489, 544, 585 and 621 nm can be assigned to $^5D_4 \rightarrow {}^7F_n$ (n = 6, 5, 4, 3) transitions, respectively. The most intense emission, at 544 nm ($^5D_4 \rightarrow {}^7F_5$), is a magnetic dipole transition (ΔJ = ±1). Both excitation and emission spectra agree well with the spectra of a terbium-ion-doped inorganic ceramic.[22]

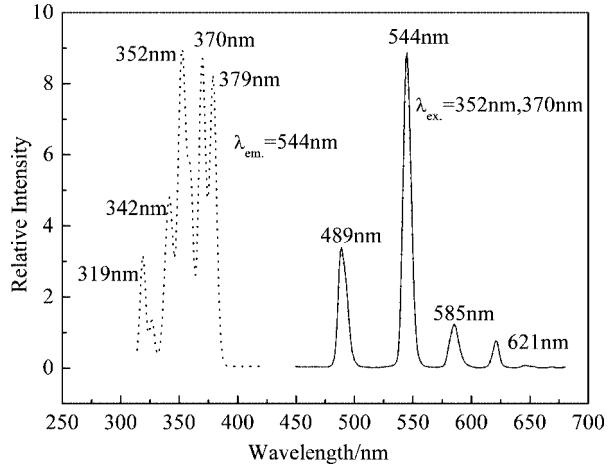

Figure 8. Excitation (dotted line) and emission (solid line) spectra of 2 in the solid state

Conclusions

Magnetic properties of the coordination frameworks in **1** and **2**, along with the fluorescence of **2**, support their structural motif. Functional carriers, such as Gd^{III} or Tb^{III} ions as the spin carriers and Tb^{III} ions as the luminescent centers, can be arranged into a special solid-state structure by the support or connection of the ligands, e.g. a 3D array of 1D chains. Such solids can display properties induced by the metals ions. Especially, the 3D framework consisting of terbium ions integrates ferromagnetic, fluorescent and porous properties into a single entity. This approach probably makes some coordination polymers promising candidates for new multifunctional molecular-based materials.

Experimental Section

Materials and Methods: All starting materials were purchased from China Medicine (Group) Shanghai Chemical Reagent Corporation and used without further purification. Elemental analyses were carried out with a Perkin–Elmer 240C elemental analyzer. IR spectra were recorded with a Bruker VECTOR22 FT-IR spectrometer using the KBr pellet technique. Thermogravimetric analyses (TGA) were performed with a TA-SDT 2960 thermal analyzer at a heating rate of 10 °Cmin^{-1} from room temperature to 600 °C under nitrogen. The solid-state excitation-emission spectrum was acquired with an AMINCO•Bowman Series AB2 Luminescence Spectrometer at room temperature. Magnetic susceptibilities were measured with a Mag Lab2000 system and a SQUID MPMS XL magnetometer. Diamagnetic corrections were made using Pascal's constants.

Syntheses and Characterization

$[Gd_2L_3(H_2O)_2]_n$ (1): A mixture of $Gd(NO_3)_3$•$6H_2O$ (45.3 mg, 0.1 mmol), succinic acid (18 mg, 0.15 mmol), NaOH (12 mg, 0.3 mmol), and H_2O (10 mL) was sealed in a 25-mL stainless-steel reactor with a Teflon liner and heated to 170 °C. After 3 d at 170 °C, the mixture was then cooled to room temperature. Colorless block-like crystals of **1** were obtained in 77.0% yield (53.8 mg) after filtration and washing with water. $C_{12}H_{16}Gd_2O_{14}$ (698.75): calcd. C 20.63, H 2.31; found C 20.62, H 2.37. IR (KBr, cm^{-1}): $\tilde{\nu}$ = 3300 (m, br.), 2983 (w), 2947 (w), 2925 (w), 2913(w), 1572 (vs, sh), 1427 (vs, sh), 1304 (s), 1215 (s), 1176 (s), 1002 (m), 909 (m), 691 (s), 652 (s), 572 (m).

$\{[TbL_{1.5}(H_2O)]\cdot 0.5H_2O\}_n$ (2): A mixture of $Tb(NO_3)_3$•$6H_2O$ (45.5 mg, 0.1 mmol), succinic acid (18 mg, 0.15 mmol), NaOH (12 mg, 0.3 mmol), and H_2O (10 mL) was sealed in a 25-mL stainless-steel reactor with Teflon liner and heated to 170 °C, kept at 170 °C for 3 d, then cooled to room temperature. Colorless block-like crystals of **2** were obtained in 69.0% yield (49.7 mg) after filtration and washed with water. $C_{12}H_{18}O_{15}Tb_2$ (720.10): calcd. C 20.02, H 2.52; found C 20.08, H 2.44. IR (KBr, cm^{-1}): $\tilde{\nu}$ = 3302 (m, br), 2983 (w), 2948 (w), 2925 (w), 2914 (w), 1576 (vs, sh), 1429 (vs, sh), 1304 (s), 1215 (s), 1176 (s), 1002 (m), 909 (m), 691 (s), 653 (s), 572 (m).

Crystallography

$[Gd_2L_3(H_2O)_2]_n$ (1): A single crystal (0.21×0.16×0.12 mm) was used for structural determination with an Enraf-Nonius CAD-4 diffractometer with graphite-monochromatized Mo-K_α radiation (λ = 0.71073) using an ω-2θ scan mode at 293 K. Intensity data were collected in the θ range 2.75–25.00°, data reduction was made with the MolEN package.[23] Absorption corrections from ψ scans were

applied. The structure was solved by direct methods using SHELXS-97 [24] and refined on F^2 by full-matrix least squares using SHELXL-97 with anisotropic displacement parameters for all non-hydrogen atoms.[25] Hydrogen atom positions were fixed geometrically at calculated distances and allowed to ride on the parent atoms. Relevant crystallographic data are presented in Table 4.

Table 4. Crystallographic data for complexes **1** and **2**

	1	**2**
Empirical formula	$C_{12}H_{16}Gd_2O_{14}$	$C_{12}H_{18}O_{15}Tb_2$
Formula mass	698.75	720.10
Crystal system	triclinic	monoclinic
Space group	$P\bar{1}$	$C2/c$
T [K]	293(2)	293(2)
a [Å]	7.7070(15)	19.919(3)
b [Å]	8.0490(16)	7.7119(11)
c [Å]	14.128(3)	13.807(2)
α [°]	96.90(3)	90
β [°]	97.03(3)	121.605(2)
γ [°]	103.25(3)	90
V [Å^3]	836.6(3)	1806.4(4)
$D_{calcd.}$ [g cm^{-3}]	2.774	2.648
Z	2	4
μ [mm^{-1}]	7.937	7.847
R_{int}	0.0204	0.0296
Reflections measured	3165	4345
Unique reflections	2928	1592
N(parameters)$_{refined}$	257	132
Goodness-of-fit on F^2	1.004	1.006
R_1 [$I > 2\sigma(I)$][a]	0.0640	0.0253
wR_2 [$I > 2\sigma(I)$][b]	0.1850	0.0581
R_1 (all data)[a]	0.0685	0.0313
wR_2 (all data)[b]	0.1914	0.0592

[a] $R_1 = \Sigma||F_o| - |F_c||/\Sigma|F_o|$. [b] $wR_2 = [\Sigma w(|F_o^2| - |F_c^2|)^2/\Sigma w(|F_o^2|)^2]^{1/2}$.

{[TbL$_{1.5}$(H$_2$O)]·0.5H$_2$O}$_n$ (2): A single crystal (0.20×0.14×0.10 mm) was used for structural determination with a Bruker SMART CCD diffractometer with graphite-monochromatized Mo-K_α radiation (λ = 0.71073) using both Φ- and ω-scan modes at 293 K. Intensity data were collected in the θ range 2.40–25.00°, data reduction was made with the Bruker SAINT package.[26] Absorption corrections were performed using the SADABS program.[27] The structure was solved by direct methods using SHELXS-97 and was refined on F^2 by full-matrix least squares using SHELXL-97 with anisotropic displacement parameters for all non-hydrogen atoms. Hydrogen atoms were introduced in calculations using the riding model. Table 4 gives the relevant crystallographic data.

CCDC-228741 (**2**) and -28742 (**1**) contain the supplementary crystallographic data for this paper. These data can be obtained free of charge at www.ccdc.cam.ac.uk/conts/retrieving.html (or from the Cambridge Crystallographic Data Centre, 12 Union Road, Cambridge CB2 1EZ, UK; Fax: +44-1223-336-033; E-mail: deposit@ccdc.cam.ac.uk).

Acknowledgments

Financial support from the National Natural Science Foundation of China and the Major State Basic Research Development Program (G200077500)the Natrual Science Foundation of China and the Natrual Science Foundation of Jangsu Province (No. BK2004414) are gratefully acknowledged. We thank Drs. Dong-Feng Li and. Tian-Wei Wang for their kind help.

[1] a) C. Janiak, *Angew. Chem. Int. Ed. Engl.* **1997**, *36*, 1431–1434; b) S. L. James, *Chem. Soc. Rev.* **2003**, *32*, 276–288.
[2] O. R. Evans, W. Lin, *Acc. Chem. Res.* **2002**, *35*, 511–522.
[3] M. Eddaoudi, D. B. Moler, H. L. Li, B. L. Chen, T. M. Reineke, M. O'Keeffe, O. M. Yaghi, *Acc. Chem. Res.* **2001**, *34*, 319–330.
[4] B. Moulton, M. J. Zaworotko, *Chem. Rev.* **2001**, *101*, 1629–1658.
[5] S. Decurtins, R. Pellaux, G. Antorrena, F. Palacio, *Coord. Chem. Rev.* **1999**, *190–192*, 841–854.
[6] C. Janiak, *J. Chem. Soc., Dalton Trans.* **2003**, 2781–2804.
[7] a) J.-C. G. Bünzli, C. Piguet, *Chem. Rev.* **2002**, *102*, 1897–1928; b) T. M. Reineke, M. Eddaoudi, M. Fehr, D. Kelley, O. M. Yaghi, *J. Am. Chem.Soc.* **1999**, *121*, 1651–1657; c) L. Ma, O. Evans, B. M. Foxman, W. Lin, *Inorg. Chem.* **1999**, *38*, 5837–5840; d) Y. J. Kim, M. Suh, D.-Y. Jung, *Inorg. Chem.* **2004**, *43*, 245–250; e) J.-M. Shi, W. Xu, Q.-Y. Liu, F.-L. Liu, Z.-L. Huang, H. Lei, W.-T. Yu, Q. Fang, *Chem. Commun.* **2002**, 756–757.
[8] a) B.-Q. Ma, D.-S. Zhang, S. Gao, T.-Z. Jin, C-.H. Yan, G.-X. Xu, *Angew. Chem. Int. Ed.* **2000**, *39*, 3644–3646; b) J.-P. Costes, F. Dahan, A. Dupuis, F. Nicodème, *Inorg. Chem.* **2001**, *40*, 5285–5287; c) R. Hedinger, M. Ghisletta, K. Hegetschweiler, E. Toth, A. E. Merbach, R. Sessoli, D. Gatteschi, V. Gramlich, *Inorg. Chem.* **1998**, *37*, 6698–6705; d) X. Zheng, C. Sun, S. Lu, F. Liao, S. Gao, L. Jin, *Eur. J. Inorg. Chem.* **2004**, 3262–3268.
[9] a) J. P. Costes, J. M. Clemente-Juan, F. Dahan, F. Nicodème, *Angew. Chem. Int. Ed.* **2002**, *41*, 323–325; b) J.-P. Costes, F. Nicodème, *Chem. Eur. J.* **2002**, *8*, 3442–3447; c) M. Hernández-Molina, C. Ruiz-Pérez, T. López, F. Lloret, M. Julve, *Inorg. Chem.* **2003**, *42*, 5456–5458; d) J.-P. Costes, J.-M. C. Juan, F. Dahan, F. Nicodème, *J. Chem. Soc.*, *Dalton Trans.* **2003**, 1272–1275; e) X.-J. Zheng, Z.-M. Wang, S. Gao, F.-H. Liao, C.-H. Yan, L.-P. Jin, *Eur. J. Inorg. Chem.* **2004**, 2968–2973.
[10] a) F. Avecilla, C. Platas-Iglesias, R. Rodríguez-Cortiñas, G. Guillemot, J.-C. G. Bünzli, C. D. Brondino, C. F. G. C. Geraldes, A. de Blas, T. Rodríguez-Blas, *J. Chem. Soc., Dalton Trans.* **2002**, 4658–4665; b) A. Dei, D. Gatteschi, C. A. Massa, L. A. Pardi, S. Poussereau, L. Sorace, *Chem. Eur. J.* **2000**, *6*, 4580–4586; c) A. W.-H. Lam, W.-T. Wong, G. Wen, X.-X. Zhang, S. Gao, *New J. Chem.* **2001**, *25*, 531–533.
[11] a) D.-L. Long, A. J. Blake, N. R. Champness, C. Wilson, M. Schröder, *Angew. Chem. Int. Ed.* **2001**, *40*, 2444–2447; b) D.-L. Long, A. J. Blake, N. R. Champness, C. Wilson, M. Schröder, *J. Am. Chem. Soc.* **2001**, *123*, 3401–3402; c) F. A. A. Paz, J. Klinowski, *Chem. Commun.* **2003**, 1484–1485; d) T. M. Reineke, M. Eddaoudi, D. Moler, M. O'Keeffe, O. M.Yaghi, *J. Am. Chem. Soc.* **2000**, *122*, 4843–4844; e) L. Pan, E. B. Woodlock, X. Wang, *Inorg. Chem.* **2000**, *39*, 4174–4178; f) V. Kiritsis, D. Michaelides, S. Skoulika, S. Golhen, L. Ouahab, *Inorg. Chem.* **1998**, *37*, 3407–3410; g) L. Pan, X. Huang, J. Li, Y. Wu, N. Zheng, *Angew. Chem. Int. Ed.* **2000**, *39*, 527–530; h) C. Serre, F. Millange, J. Marrot, G. Férey, *Chem. Mater.* **2002**, *14*, 2409–2415; i) L. Pan, N. Zheng, Y. Wu, S. Han, R. Yang, X. Huang, J. Li, *Inorg. Chem.* **2001**, *40*, 828–830; j) A. Dimos, D. Tsaousis, A. Michaelides, S. Skoulika, S. Golhen, L. Ouahab, C. Didierjean, A. Aubry, *Chem. Mater.* **2002**, *14*, 2616–2622; k) D.-L. Long, A. J. Blake, N. R. Champness, M. Schröder, *Chem. Commun.* **2000**, 1369–1370.
[12] a) C. Livage, C. Egger, G. Férey, *Chem. Mater.* **2001**, *13*, 410–414; b) C. Livage, C. Egger, G. Férey, *Chem. Mater.* **1999**, *11*, 1546–1550; c) P. M. Forster, A. R. Burbank, C. Livage, G. Férey, A. K. Cheetham, *Chem. Commun.* **2004**, 368–369; d) Y. J. Kim, D. Y. Jung, *Bull. Korean Chem. Soc.* **1999**, *20*, 827–830.
[13] a) P. M. Forster, A. K. Cheetham, *Angew. Chem. Int. Ed.* **2002**, *41*, 457–459; b) N. Guillou, C. Livage, W. van Beek, M. Nogues, G. Férey, *Angew. Chem. Int. Ed.* **2003**, *42*, 643–647.

[14] J. Perles, M. Iglesias, C. Ruiz-Valero, N. Snejko, *Chem. Commun.* **2003**, 346–347.
[15] a) F. Serpaggi, G. Férey, *Microporous Mesoporous Mater.* **1999**, *32*, 311–318; b) M. Fleck, *Z. Kristallogr. NCS* **2002**, *217*, 569–570.
[16] J.-C. G. Bünzli, G. R. Chopin, *Lanthanide Probes in Life, Chemical and Earth Sciences: Theory and Practice*, Elsevier, Amsterdam, **1989**.
[17] M. T. Hutchings, R. J. Birgeneau, W. P. Wolf, *Phys. Rev.* **1968**, *168*, 1026–1044.
[18] R. S. Meltzer, H. W. Moos, *Phys. Rev. B* **1972**, *6*, 264–277.
[19] S. Hüfner, *Optical Spectra of Transparent Rare Earth Compounds*, Academic Press, NewYork, **1978**.
[20] C. Benelli, D. Gatteschi, *Chem. Rev.* **2002**, *102*, 2369–2387.
[21] a) N. Ishikawa, T. Iino, Y. Kaizu, *J. Am. Chem. Soc.* **2002**, *124*, 11440–11447; b) N. Ishikawa, M. Sugita, T. Ishikawa, S. Koshihara, Y. Kaizu, *J. Am. Chem. Soc.* **2003**, *125*, 8694–8695.
[22] C. H. Kam, S. Buddhudu, *Mater. Lett.* **2002**, *54*, 337–342.
[23] C. K. Fair, *MolEN, Structure solution procedures*, Enraf–Nonius, Delft, **1990**.
[24] G. M. Sheldrick, *SHELXS-97, Program for crystal structure solution*, University of Göttingen, **1990**.
[25] G. M. Sheldrick, *SHELXL-97, Program for the refinement of crystal structure from diffraction data*, University of Göttingen, **1997**.
[26] G. M. Sheldrick, *SAINT+, Data integration software*, ver. 6.02a, Bruker AXS Inc., Madison, WI, **1997**.
[27] G. M. Sheldrick, *SADABS, Empirical absorption correction program*, ver. 2.01, University of Göttingen, **1996**.

Received May 7, 2004

